

## Elastic strain of freely suspended single-wall carbon nanotube ropes

D. A. Walters,<sup>a)</sup> L. M. Ericson, M. J. Casavant, J. Liu, D. T. Colbert, K. A. Smith, and R. E. Smalley

Center for Nanoscale Science and Technology and Departments of Chemistry and Physics, Rice University, Houston, Texas 77251-1892

(Received 10 February 1999; accepted for publication 28 April 1999)

We have induced large elastic strains in ropes of single-wall carbon nanotubes, using an atomic force microscope in lateral force mode. Freely suspended ropes were observed to deform as elastic strings with tension proportional to elongation. Ropes were elastically deformed over  $>10$  cycles without showing signs of plastic deformation. The maximum strain observed,  $5.8 \pm 0.9\%$ , gives a lower bound of  $45 \pm 7$  GPa for the tensile strength (specifically, yield stress) of single-wall nanotube ropes. © 1999 American Institute of Physics. [S0003-6951(99)04325-9]

Because of their structural perfection and strong carbon-carbon bonds, single-wall carbon nanotubes (SWNT) are widely expected to have high strength, making them excellent candidates for reinforcement fibers in composite materials and for high-strength cables. While large bending<sup>1-5</sup> and tensile<sup>6</sup> strains have been observed for multiwall nanotubes, few studies have considered SWNT, although breakage of SWNT has been observed in the transmission electron microscope<sup>7</sup> and atomic force microscope (AFM).<sup>8</sup> Taking inspiration from the use of the AFM to manipulate multiwall nanotubes on surfaces,<sup>3-5</sup> we have used an AFM to directly apply and measure tensile strain in ropes of SWNT. As in the elastic modulus measurements of Salvétat *et al.*,<sup>9</sup> we apply forces to a length of rope that is freely suspended across a hole or trench, so as to avoid adhesion between the nanotubes and an underlying substrate.

Single-wall carbon nanotubes were grown by pulsed laser vaporization<sup>10</sup> and purified.<sup>11</sup> The product consisted of SWNT ropes containing tens to hundreds of SWNT bound in van der Waals contact. These ropes were suspended in *N,N*-dimethylformamide. Clean silicon chips with a 100 nm thermal oxide layer were treated with 3-aminopropyltriethoxysilane, then dipped in the SWNT suspension to adhere nanotube ropes to the amine-terminated surface.<sup>12,13</sup> The rope-covered surface [Fig. 1] was masked using a copper grid as a shadow mask. Chromium (2 nm) and gold (20–50 nm) were sequentially evaporated through the mask to form pads that pinned SWNT ropes to the surface. Alternatively, pads were formed using electron-beam lithography.

The regions of oxide not covered by the pads were etched in 4.9% HF to expose the silicon, which was then anisotropically etched to a depth of 0.5–1.5  $\mu\text{m}$  in 38 wt. % KOH. This process left individual ropes freely suspended across trenches between the metal pads. In order to prevent adhesion of the suspended ropes to the walls of the trenches, the chip was rinsed with water, isopropyl alcohol, acetone, and tetramethylsilane, keeping the chip fully immersed at all times. The chip was then removed into air from tetramethylsilane, a solvent with a low surface tension (10.2 mN/m).

This dehydration procedure is used for drying biological samples as an alternative to critical point drying.<sup>14</sup>

Scanning electron microscope (SEM) images [Fig. 2(a)] reveal some freely suspended nanotube ropes to be nearly perpendicular to trenches. To apply and measure strains in such a rope, the chip was mounted in an AFM with lateral force capability.<sup>15</sup> An AFM probe tip was positioned near the suspended rope such that the tip hovered about 100 nm above the trench floor. The tip was scanned in a line parallel to the axis of the trench at 1 cycle/s with an amplitude of 1–2.5  $\mu\text{m}$ . The scan center was advanced along the trench in 50 nm increments until a lateral force signal was detected. Lateral force versus tip position was then captured for 8 to 16 scans before advancing the tip further. Advancing the scan center and capturing data continued until the rope broke [Fig. 2(b)] or detached from its endpoints. Figure 3(a) shows a typical set of lateral force curves for four consecutive tip scans about the same scan center. The measurement is highly reproducible, with no hysteresis or offset between cycles; this is evidence that the rope is neither plastically deforming nor slipping out of its attachments. In all cases analyzed

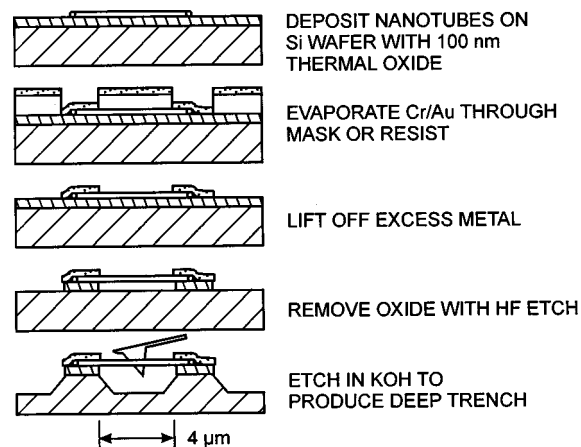


FIG. 1. Ropes of single-wall nanotubes were pinned beneath metal pads on an oxidized silicon surface, then released by wet etching. To prevent ropes from adhering to the trench walls, the sample was transferred to a low-surface-tension liquid, tetramethylsilane, and removed from liquid through its surface.

<sup>a)</sup>Electronic mail: walters@rice.edu

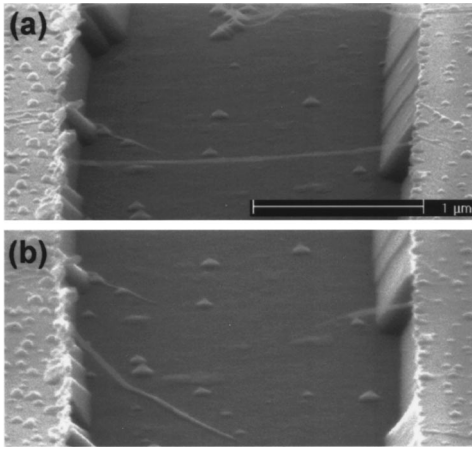


FIG. 2. Rope of single-wall nanotubes freely suspended over trench in silicon before (a) and after (b) being stressed past its elastic limit.

here, no plastic deformation or slippage was observed before or during the lateral force curves analyzed.

To model the stretched rope [Fig. 3(b)], we treat it as an elastic string with extensional spring constant  $k$  and tension  $T = k(L - L_0)$ , where  $L$  is its stretched length and  $L_0$  is its unstretched length, both measured from the points of attachment. Consider first the simplified case with the AFM tip centered on the trench ( $y_{\text{off}} = 0$ ) and the tube suspended perpendicular to the trench ( $\alpha = 0$ ). Then, we have  $L_0 = g$  and  $L = \sqrt{g^2 + 4x^2}$ , where  $g$  is the width of the trench and  $x$  is the tip position relative to the point of first contact with the tube. Therefore  $T = k(\sqrt{g^2 + 4x^2} - g)$ . Equilibrium yields a force on the AFM tip of

$$F = 2T \sin(\theta) = 2T \frac{2x}{L} = 8kx \left( \frac{x}{g} \right)^2 + \mathcal{O} \left( \frac{x}{g} \right)^4. \quad (1)$$

In the more general case of  $\alpha \neq 0$  and  $y_{\text{off}} \neq 0$ , we obtain the full expression

$$F = k \left( L_+ + L_- - \frac{g}{\cos \alpha} \right) \left( \frac{2x + g_+ \sin \alpha}{2L_+} + \frac{2x - g_- \sin \alpha}{2L_-} \right), \quad (2)$$

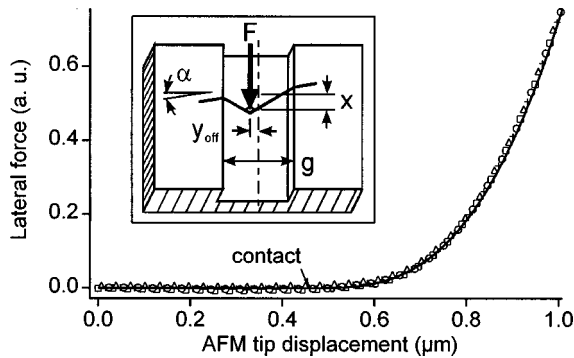


FIG. 3. (a) Lateral force on single-wall nanotube rope as a function of AFM tip position. The four symbols represent data from four consecutive lateral force curves on the same rope, showing that this rope is straining elastically with no plastic deformation. The force increases as  $x^3$  after contact, as expected for an elastic string with no slack. The solid line is a fit of Eq. (2) to the curve marked with circles. The fit parameters correspond to elastic strain of  $2.8 \pm 0.4\%$ . A linear background was subtracted from the data before fitting; only one in eight data points is shown for clarity. (b), inset. The AFM tip moves along the trench, in the plane of the surface, and displaces the rope as shown. Variables marked are used in Eq. (2).

TABLE I. Trench widths, angles, offsets, maximum extension of AFM tip, and observed elastic strains for four ropes tested. The dominant error in strain is due to calibration of the piezoelectric AFM scanner.

$g$ ( $\mu\text{m}$ )	$\alpha$ ( $^\circ$ )	$y_{\text{off}}$ ( $\mu\text{m}$ )	$x_{\text{max}} - x_0$ ( $\mu\text{m}$ )	$\epsilon_{\text{max}}$
4.3	$0^\circ$	0.26	$0.54 \pm 0.03$	$2.8 \pm 0.4\%$
3.7	$12^\circ$	0.95	$0.57 \pm 0.03$	$5.8 \pm 0.9\%$
4.1	$0^\circ$	0.67	$0.31 \pm 0.02$	$1.2 \pm 0.2\%$
4.5	$0^\circ$	0.48	$0.32 \pm 0.02$	$1.1 \pm 0.1\%$

with

$$g_{\pm} = \frac{g \pm 2y_{\text{off}}}{\cos \alpha}$$

and

$$L_{\pm} = \sqrt{g_{\pm}^2/4 + x^2 \pm g_{\pm} x \sin \alpha}.$$

In these models,  $F \propto x^3$  near  $x = 0$ . This gradual onset of force results from two factors: the tension in the rope acts nearly perpendicular to the tip motion, contributing a factor of  $x$ , and the change in length is initially of order  $x^2$ . The curves of Fig. 3(a) show that this rope does behave like an elastic string rather than a stiff beam, for which we expect  $F \propto x$  immediately after contact.<sup>16</sup> For ropes intermediate between an elastic string (all strain energy goes into stretching) and a stiff beam (all strain energy goes into bending), a sum of linear and cubic terms would be expected. Another model, an elastic string with slack, also predicts a sharp onset of  $F \propto x$ . Due to the challenge of distinguishing a rope with slack from a stiff beam, we have chosen to study ropes that have negligible slack.

The maximum elastic strain  $\epsilon_{\text{max}}$  was found using the elastic string model. A linear background was fit to the out-of-contact region of each lateral force curve and then subtracted from the entire curve. The in-contact region was then fit to Eq. (2) using measured parameters  $g$ ,  $\alpha$ , and  $y_{\text{off}}$ . Offsets in  $x$  and  $F$  were also included in the fit. As can be seen in Fig. 3(a), the fit quality is excellent. This fit was used to determine the  $x$  position at which the rope began to strain,  $x_0$ . Geometry then gives  $\epsilon_{\text{max}} = g^{-1}(L_+ + L_-) \cos \alpha$ , where  $L_{\pm}$  are evaluated at  $x = x_{\text{max}} - x_0$ , and  $x_{\text{max}}$  is the most extreme  $x$  position before breakage or plastic deformation of the rope. The tip position was corrected for the nonzero lateral compliance of the AFM tip due to cantilever bending and twisting, using the vertical and lateral deflections recorded at  $x_{\text{max}}$ . The dominant errors contributing to  $\epsilon_{\text{max}}$  are then the calibration and nonlinearity of the piezoelectric AFM scanner, from which we interpret all distance measurements. We estimate their combined effect to be less than 5% of  $(x_{\text{max}} - x_0)$ . Other errors that contribute noticeably are in  $g$  ( $\pm 3\%$ ) and  $y_{\text{off}}$  ( $\pm 100$  nm). Statistical error in determining  $x_0$  from the fit to Eq. (2) was typically negligible.

Table I lists the maximum elastic strain measured for each of four nanotube ropes. There are many potential reasons why a rope might fail at a lower strain than an individual, perfect nanotube, namely: (a) the rope might consist of overlapping nanotubes that do not span the full width of the trench, in which case the forces between adjacent tubes may be limiting; (b) the rope might fail by slipping out of or breaking its points of attachment; (c) the nanotubes in the rope might contain pre-existing defects, e.g. due to irradiation.

tion with the beam of the SEM; (d) bending of the rope at the AFM tip or the endpoints might nucleate defects prematurely at these locations;<sup>17,18</sup> (e) if the rope had a smaller diameter over some portion of its length, that portion would undergo higher strain than the average strain calculated here. Therefore our measurements provide only a lower bound on the mechanical properties of a perfect individual SWNT. Each measurement represents an *independent* lower bound. Thus the maximum of the observed strain values, not the average, is relevant:  $5.8 \pm 0.9\%$ .

Various theoretical predictions have been made regarding the strength of SWNT.<sup>17–20</sup> They agree that the maximum elastic strain and the mode of failure (brittle versus ductile) depend on the nanotube chirality and diameter. However, SWNT in the diameter range produced by laser vaporization (1.1–1.4 nm) are expected to be energetically stable against the formation of pentagon-heptagon defects at strains less than 5%. Depending on the activation barriers to defect formation, SWNT may be kinetically stable at strains of 10%–20%.<sup>21</sup> Therefore the elastic strains reported here, up to 5.8%, are consistent with current theoretical understanding. Using a Young's modulus of 1.25 TPa for single-wall carbon nanotubes,<sup>22</sup> the present results indicate that close-packed nanotube ropes will have a yield strength exceeding  $45 \pm 7$  GPa. This is over 20 times the yield strength of typical high-strength steels.<sup>23</sup>

The authors are pleased to acknowledge the assistance of Dr. A. Rimborg, M. Cox, and W. Lu with electron-beam lithography. For financial support, we gratefully thank the National Science Foundation, the Welch Foundation, and the National Aeronautics and Space Administration.

- <sup>1</sup>O. Lourie, D. M. Cox, and H. D. Wagner, *Phys. Rev. Lett.* **81**, 1638 (1998).
- <sup>2</sup>S. Iijima, C. Brabec, A. Maiti, and J. Bernholc, *J. Chem. Phys.* **104**, 2089 (1996).
- <sup>3</sup>T. Hertel, R. Martel, and P. Avouris, *J. Phys. Chem. B* **102**, 910 (1998).
- <sup>4</sup>M. R. Falvo, G. J. Clary, R. M. Taylor, V. Chi, F. P. Brooks, S. Washburn, and R. Superfine, *Nature (London)* **389**, 582 (1997).
- <sup>5</sup>E. W. Wong, P. E. Sheehan, and C. M. Lieber, *Science* **277**, 1971 (1997).
- <sup>6</sup>H. D. Wagner, O. Lourie, Y. Feldman, and R. Tenne, *Appl. Phys. Lett.* **72**, 188 (1998).
- <sup>7</sup>O. Lourie and H. D. Wagner, *Appl. Phys. Lett.* **73**, 3527 (1998).
- <sup>8</sup>J. Kong, H. T. Soh, A. M. Cassell, C. F. Quate, and H. J. Dai, *Nature (London)* **395**, 878 (1998).
- <sup>9</sup>J. P. Salvetat, G. A. D. Briggs, J. M. Bonard, R. R. Bacsa, A. J. Kulik, T. Stockli, N. A. Burnham, and L. Forro, *Phys. Rev. Lett.* **82**, 944 (1999).
- <sup>10</sup>A. Thess, R. Lee, P. Nikolaev, H. J. Dai, P. Petit, J. Robert, C. H. Xu, Y. H. Lee, S. G. Kim, A. G. Rinzler, D. T. Colbert, G. E. Scuseria, D. Tomanek, J. E. Fischer, and R. E. Smalley, *Science* **273**, 483 (1996).
- <sup>11</sup>A. G. Rinzler, J. Liu, H. Dai, P. Nikolaev, C. B. Huffman, F. J. Rodriguez-Macias, P. J. Boul, A. H. Lu, D. Heymann, D. T. Colbert, R. S. Lee, J. E. Fischer, A. M. Rao, P. C. Eklund, and R. E. Smalley, *Appl. Phys. A: Solids Surf.* **67**, 29 (1998).
- <sup>12</sup>J. Liu, M. J. Casavant, M. Cox, D. A. Walters, P. Boul, W. Lu, A. J. Rimborg, K. A. Smith, D. T. Colbert, and R. E. Smalley, *Chem. Phys. Lett.* **303**, 125 (1999).
- <sup>13</sup>M. Burghard, G. Duesberg, G. Philipp, J. Muster, and S. Roth, *Adv. Mater.* **10**, 584 (1998).
- <sup>14</sup>S. Dey, T. S. Basu Baul, B. Roy, and D. Dey, *J. Microsc.* **156**, 259 (1989).
- <sup>15</sup>Nanoscope III; Digital Instruments, Santa Barbara, CA.
- <sup>16</sup>W. Griffel, *Handbook of Formulas for Stress and Strain* (Frederick Ungar, New York, 1966).
- <sup>17</sup>B. I. Yakobson, *Appl. Phys. Lett.* **72**, 918 (1998).
- <sup>18</sup>P. H. Zhang, P. E. Lammert, and V. H. Crespi, *Phys. Rev. Lett.* **81**, 5346 (1998).
- <sup>19</sup>M. B. Nardelli, B. I. Yakobson, and J. Bernholc, *Phys. Rev. Lett.* **81**, 4656 (1998).
- <sup>20</sup>C. F. Cornwell and L. T. Wille, *Comput. Mater. Sci.* **10**, 42 (1998).
- <sup>21</sup>M. B. Nardelli, B. I. Yakobson, and J. Bernholc, *Phys. Rev. B* **57**, R4277 (1998).
- <sup>22</sup>A. Krishnan, E. Dujardin, T. W. Ebbesen, P. N. Yianilos, and M. M. J. Treacy, *Phys. Rev. B* **58**, 14013 (1998).
- <sup>23</sup>*Marks' Standard Handbook for Mechanical Engineers*, edited by E. A. Avallone and T. Baumeister (McGraw-Hill, New York, 1996).